Original paper

Michalskiite, $Cu^{2+}Mg_3Fe^{3+}_{3.33}(VO_4)_6$, an Mg analogue of lyonsite, from the Ronneburg uranium deposit, Thuringia, Germany

Anthony R. KAMPF[1*], Jakub PLÁŠIL[2], Radek ŠKODA[3], Jiří ČEJKA[4]

[1] *Mineral Sciences Department, Natural History Museum of Los Angeles County, 900 Exposition Boulevard, Los Angeles, CA 90007, USA; akampf@nhm.org*
[2] *Institute of Physics of the CAS, v.v.i, Na Slovance 1999/2, Prague 8, 182 21, Czech Republic*
[3] *Department of Geological Sciences, Faculty of Science, Masaryk University, Kotlářská 2, 611 37, Brno, Czech Republic*
[4] *Department of Mineralogy and Petrology, National Museum, Cirkusová 1740, 193 00 Prague 9, Czech Republic*
[*] *Corresponding author*

Michalskiite (IMA2019-162), $Cu^{2+}Mg_3Fe^{3+}_{3.33}(VO_4)_6$, is a new mineral found on specimens from the dump of the Lichtenberg open pit, Ronneburg uranium mining district, Thuringia, Germany. It is a secondary mineral occurring with arcanite, epsomite, hematite and syngenite on matrix consisting of fine-grained quartz, K-feldspar and mica. It forms striated prisms and needles, elongated on [001], up to about 0.2 mm long. Crystals are brown-red with a light orange streak. They are transparent and have adamantine lustre. The mineral is brittle with curved fracture, very good {001} cleavage and a Mohs hardness of ~3½. The calculated density is 3.848 g·cm^{-3} based on the empirical formula. The new mineral is biaxial (–), with $2V_{meas}$ = 49(1)°. No pleochroism was observed. Optical orientation is X = **c**. The empirical formula of michalskiite (on the basis of 24 O *apfu*) is $(Cu^{2+}_{1.33}Mg_{2.76}Fe^{3+}_{2.75}Al_{0.21}Ni_{0.16}Ti^{4+}_{0.14}Mn^{3+}_{0.06}Zn_{0.01})_{\Sigma 7.40}(V^{5+}_{5.96}Si_{0.02})_{\Sigma 5.98}O_{24}$. The Raman spectrum is dominated by the vibrations of VO_4^{3-} units. Michalskiite is orthorhombic, *Pmcn*, a = 10.2356(9), b = 17. 3689(16), c = 4.9406(4) Å, V = 878.35(13) Å^3 and Z = 2. The five strongest powder X-ray diffraction lines are [d_{obs}, Å (I, %) (*hkl*)]: 3.27 (100) (221,150), 2.74 (40) (241,151), 2.52 (50) (331), 1.55 (30) (282), 1.42 (25) (063). The crystal structure of michalskiite was refined from the single-crystal X-ray data to R = 0.0386 for 888 independent observed reflections, with $I_{obs} > 2\sigma(I)$. Michalskiite is isostructural with lyonsite; however, the Cu2 site in the lyonsite structure is split into *M*2 and *M*2' sites in the michalskiite structure with Mg occupying the *M*2' site. The new mineral name honours German mineral collector and dealer Dipl. Min. Steffen Michalski, who discovered this mineral.

Keywords: michalskiite, new mineral, lyonsite, crystal structure, Raman spectroscopy
Received: 25 January 2022; accepted: 4 April 2022; handling editor: F. Laufek
The online version of this article (doi: 10.3190/jgeosci.341) contains supplementary electronic material.

1. Introduction

Nearly 25 years ago, a new mineral, lyonsite, $Cu_3Fe_4(VO_4)_6$, was described as a fumarolic sublimate from Izalco volcano in El Salvador (Hughes et al. 1987). In 2011, pseudolyonsite, $Cu_3(VO_4)_2$ (Zelenski et al. 2011) was described from the famous Tolbachik volcano in Kamchatka Peninsula (Russian Federation). Here, we report on the new mineral michalskiite, an Mg-analogue of lyonsite, found in a completely different geological environment – it is a secondary alteration product probably formed at low temperature under oxidizing conditions in the uranium deposit at Ronneburg in Thuringia, Germany.

Michalskiite is named for Dipl. Min. Steffen Michalski (born June 1, 1974). Mr. Michalski is a well-known mineral collector and dealer focused mainly on minerals from Saxony. He is also a co-author of several papers and articles focused on mineralogy (e.g. Michalski et al. 2002; Massanek et al. 2018). He discovered the new mineral and provided the holotype specimen.

The new mineral and the name have been approved by the International Mineralogical Association (IMA2019-062). The description of the new mineral is based on one holotype specimen deposited in the collections of the Natural History Museum of Los Angeles County, 900 Exposition Boulevard, Los Angeles, CA 90007, USA, catalogue number 67614.

2. Occurrence

Michalskiite has been found on very few specimens, all of which originate from the dump of the Lichtenberg open-pit (50°51'20.0'' N 12°09''58.0'' E), Ronneburg mining district, Thuringia, Germany. Specimens originate from the same area as those bearing the rare vanadate ronneburgite (Witzke et al. 2001). Between 1949 and 1990, about 7 % of the total world production of uranium came from the Ronneburg deposit; it was the most productive uranium minefield in all of Europe. A total of

112,914 tonnes of U was produced during this period. The Lichtenberg open pit was active during the period 1958–1977. The uranium mineralization is deposited in Ordovician, Silurian and Devonian slates, limestones and diabase; the average uranium content of the mined ore was only 0.099 %. The source of vanadium in the mineralization remains unknown; however, it is common for vanadium to be deposited along with uranium in black-shale-related deposits such as Ronneburg. More than 230 mineral species are known from the deposit; a more detailed description has been given by Witzke and Rüger (1998). Michalskiite is associated with arcanite (identification based on EDS), epsomite, hematite and syngenite on a matrix consisting of fine-grained quartz, K-feldspar and mica. Michalskiite is presumed to be a post-mining alteration product formed at low temperature under oxidizing conditions.

3. Physical and optical properties

Michalskiite crystals are striated prisms and needles, up to about 0.2 mm long, with rectangular cross-sections. Crystal faces are sometimes rounded, appearing "melted" (Fig. 1). Crystals are elongated on [001]; no forms were measured, but {100} and {010} appear likely. Crystals are transparent with an adamantine lustre. The mineral has a light orange streak. Michalskiite is non-fluorescent under both LW and SW UV. The Mohs hardness is about 3½. Crystals are brittle with very good cleavage on {001} and have curved fracture. The calculated density is 3.848 $g \cdot cm^{-3}$ based on the empirical formula; 3.827 $g \cdot cm^{-3}$ for the ideal formula. Michalskiite is unreactive in concentrated HCl and in concentrated NaOH at room temperature.

Fig. 1 Michalskiite crystals (brown-red) with epsomite efflorescence (white) and tiny hematite crystals (black) on fine-grained quartz–feldspar–mica matrix; FOV 0.36 mm across (photo by A. Kampf).

Indices of refraction could not be measured because they are higher than available liquids; however, other optical measurements were possible and allowed the calculation of the indices of refraction based on the average index of refraction calculated using the Gladstone-Dale relation (2.150). Birefringence measurements were made using a Berek compensator: $\beta - \alpha = 0.04(1)$ and $\gamma - \alpha = 0.05(1)$. A measured $2V$ of 49(1)° was obtained from extinction data using EXCALIBRW (Gunter et al. 2004). Michalskiite is biaxial (–), $\alpha = 2.12$, $\beta = 2.16$, $\gamma = 2.17$; 2V (calc.) = 52.3°. The dispersion could not be observed. The partially determined optical orientation is $X =$ **c** (length fast). The mineral is nonpleochroic.

4. Chemical composition

Chemical analyses (10 points) were obtained on the electron microprobe Cameca SX100 (Masaryk University, Brno), operating in wavelength dispersive spectroscopy mode using an accelerating voltage of 15 kV, beam current of 20 nA and a 2 μm beam diameter. Concentrations of other elements then those reported in Tab. 1 were below detection limits (ca 0.02–0.05 wt. %). Matrix correction by PAP software (Pouchou and Pichoir 1985) was applied to the data. The empirical formula calculated on the basis of 24 O *apfu* is $(Cu^{2+}_{1.31}Mg_{2.76}Fe^{3+}_{2.75}Al_{0.21}Ni_{0.16}Ti^{4+}_{0.14}Mn^{3+}_{0.06}Zn_{0.01})_{\Sigma 7.40}(V^{5+}_{5.96}Si_{0.02})_{\Sigma 5.98}O_{24}$. The ideal formula is $Cu^{2+}Mg_3Fe^{3+}_{3.33}(VO_4)_6$ or, arranged structurally, $Fe^{3+}_{1.33}(Cu^{2+}Mg)(Fe^{3+}Mg)_2(VO_4)_6$, which requires CuO 7.86, MgO 11.95, Fe_2O_3 26.27, V_2O_5 53.92, total 100 wt. %.

Tab. 1 Chemical composition (in wt. %) for michalskiite

Constituent	Mean	Range	S.D.	Standard
ZnO	0.07	0.02–0.14	0.04	gahnite
CuO	10.10	9.83–10.33	0.15	lammerite
MgO	10.80	10.72–10.87	0.05	Mg_2SiO_4
NiO	1.16	1.05–1.30	0.07	Ni_2SiO_4
TiO_2	1.09	1.05–1.16	0.03	titanite
Mn_2O_3	0.49	0.46–0.52	0.02	spessartine
Al_2O_3	1.05	1.01–1.10	0.03	sanidine
Fe_2O_3	21.39	21.18–21.87	0.21	andradite
V_2O_5	52.72	52.37–53.05	0.23	$ScVO_4$
SiO_2	0.12	19.02–20.07	0.02	sanidine
Total	98.99			

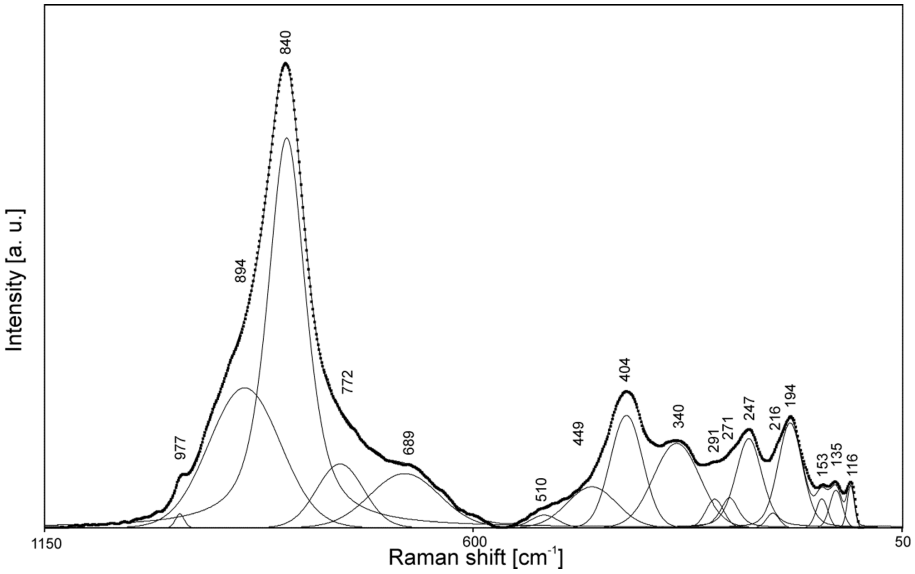

Fig. 2 Raman spectrum of michalskiite.

5. Raman spectroscopy

The Raman spectrum of michalskiite (Fig. 2) was collected on a HORIBA Jobin Yvon LabRAM HR spectrometer, using a grid of 600 gratings/mm, 100× objective and a 633 nm laser. The Raman modes were tentatively assigned based on Nakamoto (2009) and inferred especially from the papers by Frost et al. (2001, 2005, 2011) and Dordević et al. (2016). The spectrum was essentially featureless from 4000–1100 cm^{-1}, indicating that the mineral is anhydrous.

Ideally, the VO_4^{3-} ion belongs to the point group T_d. If one classifies molecular vibrations, the total reducible representation decomposes into $\Gamma = A_1 + E + 2F_2$. Infrared and Raman wavenumbers for these four fundamental modes are as follows: ν_1 (A_1) symmetric stretching vibration (Raman active) 826 cm^{-1}; ν_2 (δ) (E) doubly degenerate bending vibration (Raman active) 336 cm^{-1}; ν_3 (F_2) triply degenerate antisymmetric vibration (infrared and Raman active) 804 cm^{-1}, ν_4 (δ) (F_2) triply degenerate bending vibration (infrared and Raman active) 336 cm^{-1} (Nakamoto 2009). The lowering of the symmetry due to the crystal field (site and the factor group symmetry) leads to the splitting of degenerate vibrations and activation of the forbidden modes in Raman (for instance ν_2) or infrared (for instance ν_1).

A very strong band at 840 cm^{-1} is attributed to the ν_1 VO_4^{3-} symmetric stretching vibration. Bands at 977, 894 (shoulder) and 772 (shoulder) cm^{-1} are assigned to the split triply degenerate ν_3 VO_4^{3-} antisymmetric stretching vibrations; however, the assignment of the band at 977 cm^{-1} is problematic. In some complexly polymerized vanadium phases and especially in the case of uranyl-vanadate minerals and their synthetic analogues, this vibration may be Raman and infrared active and is connected with the ν_1 VO_3^- symmetric stretching vibration in (V_2O_2) units (Frost et al. 2005). According to Wilkins (1971), it

Tab. 2 Powder X-ray data (d in Å) for michalskiite. Only calculated lines with $I > 1.5$ are shown

I_{obs}	d_{obs}	I_{calc}	d_{calc}	h	k	l
5	5.28	29	5.12	1	1	0
10	4.46	8	4.41	2	2	0
5	3.51	10	3.52	1	3	1
100	3.27	100	3.29	2	2	1
		32	3.29	1	5	0
20	3.20	15	3.26	1	4	1
20	2.90	7	2.94	3	3	0
		5	2.90	0	6	0
15	2.80	11	2.77	3	1	1
40	2.74	10	2.75	2	4	1
		17	2.74	1	5	1
50	2.52	30	2.53	3	3	1
15	2.44	13	2.47	0	0	2
5	2.08	6	2.08	2	3	2
5	2.00	3	2.01	0	5	2
5	1.95	5	1.95	3	2	2
15	1.89	12	1.89	3	3	2
5	1.81	2	1.82	3	4	2
15	1.78	6	1.79	4	6	1
8	1.67	6	1.68	3	9	0
10	1.58	2	1.59	6	4	0
		9	1.59	6	2	1
30	1.55	7	1.55	2	8	2
8	1.53	1	1.53	5	3	2
10	1.48	3	1.49	1	11	1
25	1.42	3	1.43	0	6	3
5	1.38	3	1.39	3	9	2
2	1.36	4	1.36	7	3	1

is possible that structures with isolated VO_4^{3-} tetrahedra are atypical amongst the uranyl vanadates. Condensed vanadate ions are also consistent with the presence of strong vanadate infrared absorption bands well outside the range expected for isolated VO_4^{3-} tetrahedra.

A weak very, broad band at 689 cm^{-1} may be attributable to V–O stretching (Hardcastle and Wachs 1991) and a very weak, broad band at 600 cm^{-1} with stretching vibrations of M^{3+} octahedra. A band of medium intensity at 404 cm^{-1} with shoulders at 510 and 449 cm^{-1} is assigned to the split ν_4 (δ) VO_4^{3-} triply degenerate bending vibrations and a broad, weak band at 340 cm^{-1} is assigned to the doubly degenerate ν_2 (δ) VO_4^{3-} bending vibrations.

A weak medium strong band at 247 cm^{-1} with shoulders at 291, 271 and 216 cm^{-1} may be attributed to *M*–O stretching vibrations of M^{3+}–O and M^{2+}–O involved in octahedral, trigonal prismatic and square-planar coordinations, as described in the crystal structure section below. Weak and very weak bands at 194, 153, 135 and 116 cm^{-1} may be assigned to lattice modes (Hughes et al. 1987; Čejka et al. 2015; Jirásek et al. 2017; Xiao et al. 2018).

6. Powder X-ray diffraction

X-ray powder diffraction data were recorded using a Rigaku SuperNova diffractometer with Atlas S2 CCD detector and monochromatized Mo*K*α radiation from the microfocus X-ray tube. A Gandolfi-like motion on the φ and ω axes was used to randomize the sample. Because the quality of the observed diffraction pattern was not good enough to perform profile fitting, observed d_{hkl} values were obtained by the peak-search routine in the High-Score software (PANalytical, Almelo, B.V.). In Tab. 2, the observed data are compared with the values calculated from the structure data using the program PowderCell (Kraus and Nolze 1996).

7. Single-crystal X-ray diffraction

The single-crystal X-ray study was done on a Rigaku SuperNova diffractometer with mirror–monochromatized MoK_α radiation (λ = 0.71073 Å) from a microfocus X-ray source detected by an Atlas S2 CCD detector. The CrysAlis Pro software package was used for processing the structure data, including the application of an empirical absorption correction using the multi-scan method with ABSPACK3. SHELXL-2016 (Sheldrick 2015) was used for the refinement of the structure with initial atom coordinates taken from the structure of lyonsite (Hughes et al. 1987), with which michalskiite is isostructural. The lyonsite Cu2 site was found to be split into two sites, one at essentially the same position as in lyonsite (designated *M*2) and one displaced from it by 0.45 Å (designated *M*2'). The cation-site assignments and occupancies were analyzed using *OccQP* (Wright et al. 2001), which uses quadratic equations in a constrained least-squares formulation to optimize occupancy assignments based upon site scattering, chemical composition, charge balance, bond valence and cation-anion bond lengths. In our analysis, we assumed the lyonsite Cu1 site (designated *M*1) to have variable occupancy, the *M*2 and *M*2' sites to have a total occupancy of 1 (full), and the lyonsite Fe3 site (designated *M*3) and the two V sites (V1 and V2 to have full occupancies. Data collection and refinement details are given in Tab. 3, atom coordinates and displacement parameters in Tab. 4, cation site assignments in Tab. 5, selected bond distances in Tab. 6 and a

Tab. 3 Data collection and structure refinement details for michalskiite

Diffractometer	Rigaku SuperNova with Atlas S2 CCD
X-ray radiation/power	Mo*K*α (λ = 0.71075 Å)/40 kV, 30 mA
Temperature	293 K
Structural Formula*	$(Fe_{0.606})_2(Cu_{0.58})_2(Mg_{0.47})_2(Fe_{0.467}Mg_{0.533})_4(V_{0.955})_2(V_{0.971})_4O_{24}$
Space group	*Pmcn*
Unit cell dimensions	*a* = 10.2356(9) Å
	b = 17.3689(16) Å
	c = 4.9406(4) Å
V	878.35(13) Å^3
Z	2
Density (for above formula)	3.777 g cm^{-3}
Absorption coefficient	7.00 mm^{-1}
F(000)	951.2
Crystal size	68 × 33 × 20 μm
θ range	3.98 to 28.32°
Index ranges	$-12 \le h \le 13$, $-22 \le k \le 20$, $-6 \le l \le 6$
Reflections collected/unique	4947/1052; R_{int} = 0.050
Reflections with $I > 2\sigma I$	888
Completeness to θ = 28.32°	90.8%
Refinement method	Full-matrix least-squares on F^2
Parameters/restraints	106/0
GoF	1.121
Final *R* indices [$I > 3\sigma I$]	*R* = 0.0386, *wR* = 0.0781
R indices (all data)	*R* = 0.0484, *wR* = 0.0834
Largest diff. peak/hole	+1.01/–1.22 e A^{-3}

* Based on refined cation-site occupancies that were used in *OccQP* analysis.

bond-valence analysis in Tab. 7. The crystallographic information file (cif) for michalskiite is provided as Supplementary material.

As noted above, michalskiite is isostructural with lyonsite (a short comparison given in Tab. 8), the structure of which was solved and described in detail by Hughes et al. (1987). The structure (Fig. 3) is based on a pseudohexagonal close-packed array of O atoms (with the pseudo-6-fold axis parallel to [001]. V^{5+} cations occupy tetragonal interstices arranged in a pinwheel fashion around a column of face-sharing *M*1 octahedra. This column extends along [001], as do edge-sharing *zig–zag* chains of *M*2 trigonal prisms and *M*3 octahedra. As is the case in lyonsite, adjacent *M*1 sites across the shared octahedral face are generally too close together (2.47 Å) to be occupied simultaneously. Site scattering refinement combined with *OccQP* analysis showed this site to be occupied by $Fe^{3+}_{0.389}Cu^{2+}_{0.200}$. The total *M*1 occupancy of 0.589 is essentially the same as that found in lyonsite (0.59; all Cu) and suggests that adjacent *M*1 sites are sometimes occupied. The *OccQP* calculated occupancy may, in fact, be somewhat underestimated because it yields significantly low bond-valence sums (BVS) for the coordinated O atoms (O1 and O6). In addition, the EPMA provides a somewhat greater cation total than could be accommodated without having an *M*1 occupancy of about 0.7.

An interesting difference between the lyonsite and michalskiite structures is seen in the lyonsite Cu2 site, which, as noted above, is split into two partially occupied sites (*M*2 and *M*2') in michalskiite. The *M*2 site coordinates to four O atoms (two O2 and two O7) at short distances in a square planar arrangement common for Cu^{2+} (and Ni^{2+}); however, unlike the Jahn-Teller distorted octahedral coordination typically

Tab. 4 Atom coordinates and displacement parameters (Å²) for michalskiite

	x/*a*	*y*/*b*	*z*/*c*	U_{eq}	Occupancy
*M*1	3/4	0.74918(8)	0.9085(4)	0.0324(7)	Fe 0.606(5)
*M*2	1/4	0.8223(6)	0.2109(17)	0.0081(11)	Cu 0.58(3)
*M*2'	1/4	0.801(2)	0.263(5)	0.012(3)	Mg 0.47(9)
*M*3	0.42295(8)	0.97236(5)	0.24751(14)	0.0071(3)	Mg 0.553, Fe 0.467(9)
V1	1/4	0.05663(6)	–0.22296(18)	0.0062(4)	V 0.955(7)
V2	0.47154(7)	0.84417(4)	0.72431(12)	0.0064(3)	V 0.971(6)
O1	0.6139(3)	0.79578(16)	0.6579(6)	0.0164(7)	1
O2	0.3852(3)	0.87273(15)	0.4296(5)	0.0132(7)	1
O3	1/4	0.9940(2)	0.0650(8)	0.0154(9)	1
O4	0.3847(3)	0.03502(15)	0.5849(6)	0.0149(7)	1
O5	0.5051(3)	0.92640(15)	0.9131(5)	0.0132(7)	1
O6	3/4	0.6521(2)	0.6522(8)	0.0176(10)	1
O7	0.3749(3)	0.79076(15)	–0.0759(6)	0.0164(7)	1
	U^{11}	U^{22}	U^{33}	U^{23}	U^{13}	U^{12}
*M*1	0.0053(8)	0.0117(9)	0.0801(15)	0.0106(8)	0.000	0.000
*M*2	0.0080(8)	0.012(2)	0.0046(17)	–0.0033(12)	0.000	0.000
*M*2'	0.006(3)	0.020(8)	0.010(5)	0.007(5)	0.000	0.000
*M*3	0.0066(5)	0.0101(5)	0.0044(5)	–0.0001(3)	–0.0004(3)	0.0000(3)
V1	0.0039(6)	0.0106(6)	0.0041(5)	–0.0007(4)	0.000	0.000
V2	0.0055(4)	0.0090(4)	0.0047(4)	–0.0008(2)	–0.0004(2)	0.0008(3)
O1	0.0151(16)	0.0168(15)	0.0173(16)	0.0004(12)	0.0012(13)	0.0003(13)
O2	0.0118(15)	0.0167(14)	0.0112(14)	–0.0008(11)	–0.0011(12)	–0.0011(12)
O3	0.013(2)	0.023(2)	0.011(2)	0.0018(17)	0.000	0.000
O4	0.0114(15)	0.0168(14)	0.0166(15)	–0.0030(12)	0.0015(12)	–0.0003(12)
O5	0.0118(15)	0.0165(14)	0.0111(15)	–0.0011(12)	0.0002(12)	–0.0001(12)
O6	0.010(2)	0.021(2)	0.022(2)	0.0042(19)	0.000	0.000
O7	0.0179(16)	0.0166(15)	0.0148(15)	–0.0012(12)	0.0008(12)	0.0019(12)

Tab. 5 Cation site occupancies and site scattering values for michalskiite

Site	Site Scattering Values*		*OccQP* calculated site populations
	Refinement	*OccQP*	
*M*1	63.0	63.7	$Fe^{3+}_{0.389}Cu^{2+}_{0.200}$
*M*2	67.3	66.7	$Cu^{2+}_{0.424}Ni_{0.156}$
*M*2'	22.6	20.2	$Mg_{0.420}$
*M*3	148.3	151.9	$Fe^{3+}_{0.479}Mg_{0.476}Ti^{4+}_{0.024}Al_{0.019}Mn^{2+}_{0.002}$
V1	87.9	91.3	$V^{5+}_{0.983}Al_{0.017}$
V2	178.7	182.2	$V^{5+}_{0.977}Al_{0.023}$

* Site scattering value = mean atomic number × site multiplicity.

Tab. 6 Selected bond distances (Å) for michalskiite

*M*1–O1 (×2)	2.017(3)	*M*2'–O2 (×2)	2.038(17)	V1–O6	1.695(4)
*M*1–O1 (×2)	2.032(3)	*M*2'–O7 (×2)	2.113(17)	V1–O4 (×2)	1.715(3)
*M*1–O6	2.095(4)	*M*2'–O7 (×2)	2.19(4)	V1–O3	1.791(4)
*M*1–O6	2.109(5)	<*M*2'–O>	2.114	<V1–O>	1.729
<*M*1–O>	2.050				
		*M*3–O2	1.988(3)	V2–O7	1.677(3)
*M*2–O2 (×2)	1.962(4)	*M*3–O5	2.019(3)	V2–O1	1.714(3)
*M*2–O7 (×2)	1.986(5)	*M*3–O3	2.022(2)	V2–O5	1.740(3)
*M*2–O7 (×2)	2.570(11)	*M*3–O4	2.029(3)	V2–O2	1.774(3)
<*M*2–O>	2.173	*M*3–O5	2.065(3)	<V2–O>	1.726
		*M*3–O4	2.140(3)		
		<*M*3–O>	2.044		

Tab. 7 Bond-valence analysis for michalskiite. Values are expressed in valence units (*vu*).

	*M*1	*M*2	*M*2’	*M*3	V1	V2	Σ
O1	$0.46^{\times 2\downarrow}$,$0.44^{\times 2\downarrow}$ $0.27^{\rightarrow}$,$0.26^{\rightarrow}$					1.24	1.77
O2		$0.46^{\times 2\downarrow}$ $0.27^{\rightarrow}$	$0.38^{\times 2\downarrow}$ $0.16^{\rightarrow}$	0.48		1.06	1.97
O3				$^{\downarrow}0.44^{\times 2\rightarrow}$	1.02		1.90
O4				0.44,0.33	$^{\times 2\downarrow}1.23^{\rightarrow}$		2.00
O5				0.45,0.40		1.16	2.01
O6	$0.37^{\downarrow}$,$0.36^{\downarrow}$ $0.22^{\rightarrow}$,$0.21^{\rightarrow}$				1.30		1.73
O7		$0.43^{\times 2\downarrow}$,$0.08^{\times 2\downarrow}$ $0.25^{\rightarrow}$,$0.05^{\rightarrow}$	$0.32^{\times 2\downarrow}$,$0.27^{\times 2\downarrow}$ $0.13^{\rightarrow}$,$0.11^{\rightarrow}$			1.36	1.90
Σ	2.54	1.94	1.94	2.54	4.78	4.82	

* Bond valences are based upon *OccQP* calculated cation occupancies (see Table 5). All bond-valence parameters are taken from Gagné and Hawthorne (2015). Bond valence values without arrows are summed (×1) in both directions; those with arrows and multipliers are summed as indicated.

Tab. 8 Comparison of ideal formulas, cell parameters and calculated densities (ideal) for michalskiite and lyonsite (Hughes et al. 1987)

	Michalskiite	**Lyonsite**
Ideal Formula	$Cu^{2+}Mg_3Fe^{3+}_{3.33}(VO_4)_6$	$Cu^{2+}_3Fe^{3+}_4(VO_4)_6$
Space group	*Pmcn*	*Pmcn*
a (Å)	10.2356(9)	10.296(1)
b (Å)	17.3689(16)	17.207(2)
c (Å)	4.9406(4)	4.910(1)
V (Å^3)	878.35(13)	869.87
Z	2	2
Density (g cm^{-3})	3.827	4.21

exhibited by Cu^{2+} in which two longer Cu–O bonds are in *trans* configuration, in the lyonsite and michalskiite structures, the two longer Cu–O bonds are in *cis* configuration in trigonal prismatic coordinations. The *M*2 site is located almost on one of the three square faces of the trigonal prism, while the *M*2’ site in michalskiite is displaced toward the centre of the trigonal prism providing bonds much more conducive to occupancy by Mg. BVS calculations suggest that the small amount of Zn provided by the EPMA also seems most readily accommodated at the *M*2’ site. The splitting of the *M*2 site and the resulting coordinations are shown in Fig. 4.

The remaining six-fold coordinated cation site *M*3 is fully occupied. *OccQP* calculations suggest that this site accommodates Fe^{3+}, Mg^{2+}, Al^{3+}, Ti^{4+} and Mn^{3+}, with Fe^{3+} and Mg^{2+} in almost equal amounts making up the vast majority of the site occupancy ($Fe^{3+}_{0.479}Mg^{2+}_{0.476}$). The occupancies of the two V sites refined to slightly lower than full occupancies by V alone, indicating the presence of a less strongly scattering cation(s) at the sites. *OccQP* placed some Al at each of these sites and the small amount of Si measured by EPMA is clearly accommodated in these sites.

Acknowledgement. The authors thank reviewers Juraj Majzlan and Martin Števko and handling editor František Laufek for valuable suggestions for improving the manuscript. This work was supported by the John Jago Trelawney Endowment to the Mineral Sciences Department of the Natural History Museum of Los Angeles County and by the Operational Programme of the MEYS CR (Project No. SOLID21 CZ.02. 1.01/0.0/0.0/16_019/0000760).

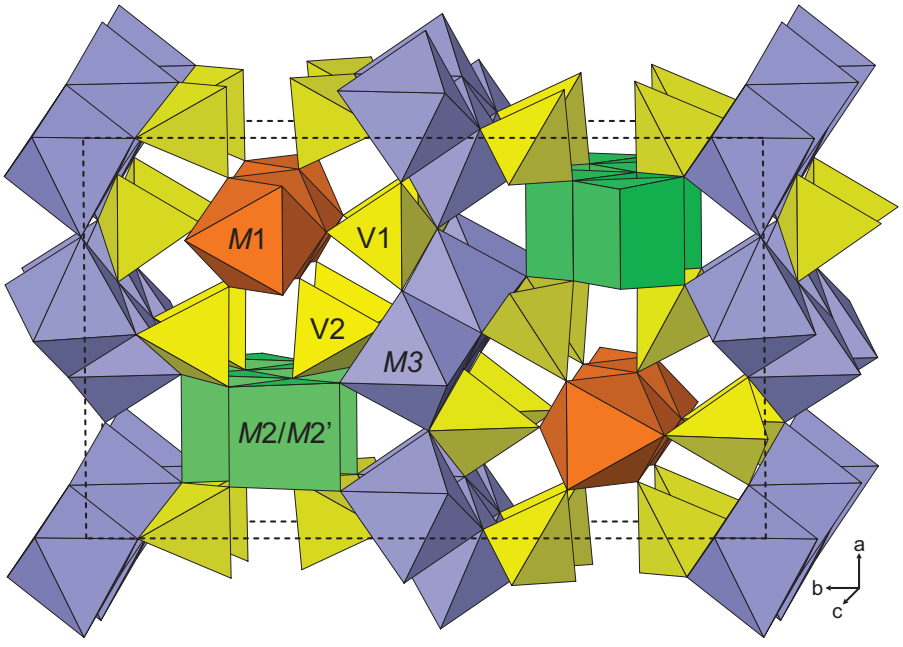

Fig. 3 The structure of michalskiite viewed slightly canted along [001]. The unit-cell outline is shown by dashed black lines.

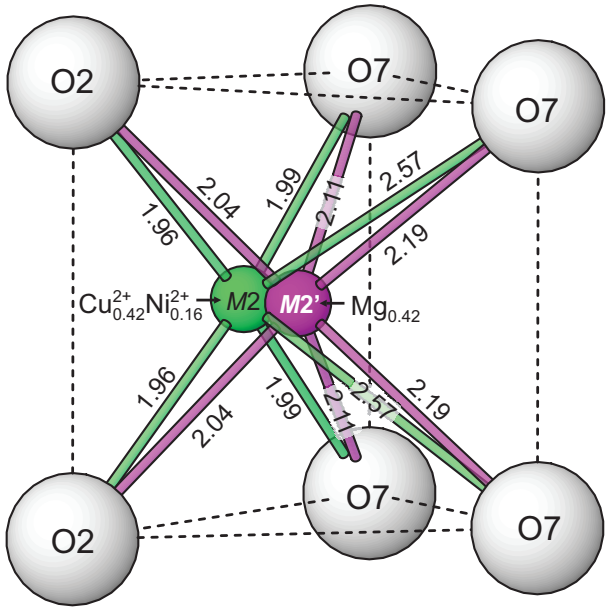

Fig. 4 Trigonal prismatic coordination surrounding the *M*2 and *M*2' sites in michalskiite.

Electronic supplementary material. Supplementary data for this paper (crystallographic information file) are available online at the Journal web site (http://dx.doi.org/10.3190/jgeosci.341).

References

Čejka J, Sejkora J, Macek I, Malíková R, Wang L, Scholz R, Xi X, Frost RL (2015) Raman and infrared spectroscopic study of turquoise minerals. Spectrochim Acta A149: 173–182

Dordević T, Kolitsch U, Nasadala L (2016) A single-crystal X-ray and Raman spectroscopic study of hydrothermally synthesized arsenates and vanadates with the decloizite and adelite structure types. Amer Miner 101: 1135–1149

Frost RL, Williams PA, Kloprogge T, Leverett P (2001) Raman spectroscopy of decloizite and mottramite at 298 and 77 K. J Raman Spectrosc 32: 906–911

Frost RL, Erickson KL, Weier ML, Carmody O (2005) Raman and infrared spectroscopy of selected vanadates. Spectrochim Acta A61: 829–834

Frost RL, Palmer SJ, Čejka J, Sejkora J, Plášil J, Bahfenne S, Keeffe EC (2011) Raman spectroscopic study of the different vanadate groups in solid-state compounds, model case: mineral phases vesigneite, $BaCu_3(VO_4)_2(OH)_2$, and volborthite, $Cu_3V_2O_7(OH)_2{\cdot}2H_2O$. J Raman Spectrosc 42: 1701–1720

Gagné OC, Hawthorne FC (2015) Comprehensive derivation of bond-valence parameters for ion pairs involving oxygen. Acta Crystallogr B71: 562–578

Gunter ME, Bandli BR, Bloss FD, Evans SH, Su SC, Weaver R (2004) Results from a McCrone spindle stage short course, a new version of EXCALIBR, and how to build a spindle stage. The Microscope 52: 23–39

Hardcastle FD, Wachs IE (1991) Determination of vanadium–oxygen bond distances and bond orders by Raman spectroscopy. J Phys Chem 95: 5031–5041

Hughes JM, Starkey SJ, Malinconico ML, Malinconico LL (1987) Lyonsite, $Cu_3Fe_4(VO_4)_6$, a new fumarolic sublimate from Izalco volcano, El Salvador: Descriptive mineralogy and crystal structure. Amer Miner 72: 1000–1005

Jirásek J, Čejka J, Vrtiška L, Matýsek D, Ruan X, Frost RL (2017) Molecular structure of the phosphate mineral koninckite – a vibrational spectroscopic study. J Geosci 62: 271–279

Kraus W, Nolze G (1996) POWDER CELL – a program for the representation and manipulation of crystal structures and calculation of the resulting X-ray powder patterns. J Appl Crystallogr 29: 301–303

Massanek A, Michalski S, Thalheim K, Herrmann S, Gebhard G, Wilson WE, Moore TP (2018) The Schneeberg mining district, Western Erzgebirge, Saxony, Germany. Mineral Rec 49: 619–742

Michalski S, Götze J, Siedel H, Magnus M, Heimann RB (2002) Investigations into provenance and properties of ancient building sandstones of the Zittau/Görlitz region (Upper Lusatia, Eastern Saxony, Germany). *In*: Siegesmund S, Vollbrecht A,Weiss T (eds) Natural stone, weathering phenomena, conservation strategies and case studies. Geological Society Special Publications, London, p 281–295

Nakamoto K (2009) Infrared and Raman spectra of inorganic and coordination compounds, Part A: Theory and applications in inorganic chemistry, 6th Ed. John Wiley & Sons, Inc., pp 1–432

Pouchou JL, Pichoir F (1985) "PAP" ϕ (ρZ) procedure for improved quantitative microanalysis. *In*: Armstrong JT (ed.) Microbeam Analysis,. San Francisco Press, California, pp 104–106

Sheldrick GM (2015) Crystal Structure refinement with *SHELX*. Acta Crystallogr C71: 3–8

Wilkins RWT (1971) Infrared spectroscopy in the mineralogical sciences of uranium ores. Neu Jb Mineral, Mitt 1971: 440–450

Witzke T, Rüger F (1998) Die Minerale der Ronneburger und Culmitzscher Lagerstätten in Thüringen. Lapis 23(7/8): 26–64

Witzke T, Zhen S, Seff K, Doering T, Nasdala L, Kolitsch U (2001) Ronneburgite, $K_2MnV_4O_{12}$, a new mineral from Ronneburg, Thuringia, Germany: Description and crystal structure. Amer Miner 86: 1081–1086

Wright SE, Foley JA, Hughes, JM (2001) Optimization of site occupancies in minerals using quadratic programming. Amer Miner 85: 524–531

Xiao RZ, Hu T, Yuan X, Zhou JJ, Na XQ, Fu DJ (2018) Studies of La- and Pr-driven reverse distortion of FeO_6 octahedral structure, magnetic properties and hyperfine interaction of $BiFeO_3$ powder. RSC Advances 22: 12060–12068

Zelenski ME, Zubkova NV, Pekov IV, Boldyreva MM, Pushcharovsky DY, Nekrasov AN (2011). Pseudolyonsite, $Cu_3(VO_4)_2$, a new mineral species from the Tolbachik volcano, Kamchatka Peninsula, Russia. Eur J Miner 23: 475–481